Computational Study of Copper Binding to DAHK peptide

Amelia Milner, Nadiyah Alshammari, James A. Platts*

School of Chemistry, Cardiff University, Park Place, Cardiff CF10 3AT, UK.

* Author for correspondence: email platts@cardiff.ac.uk, phone +44-2920-874950

Abstract

Ligand Field Molecular Mechanics (LFMM), Density Functional Theory (DFT) and Semi-Empirical methods are used to study Cu(II) binding to the tetrapeptide Asp-Ala-His-Lys (DAHK). Two conformational searching tools, LFMM/AMBER and CREST/xTB, are used to predict the energy and geometry of Cu-DAHK, using DFT as a benchmark. In addition, DFT-predicted electronic spectra are used to evaluate the binding modes found. LFMM and DFT reproduce the experimentally determined coordination, a distorted square planar arrangement of 4 nitrogen ligands with axial coordination to a fifth, oxygen ligand. However, CREST conformational search was unsuccessful in predicting the coordination mode of Cu-DAHK, changing the bonding equatorial ligands from 4N to 3N1O.

Keywords

Peptide; Copper; Conformations; Molecular Mechanics; Semi-Empirical; DFT

Introduction

Asp-Ala-His-Lys (DAHK) is a peptide, shown in Figure 1, that is found in the N-terminus of human serum albumin (HSA)[1], the most abundant protein found in blood plasma. HSA has essential functions in the distribution of transition metal ions, oxygen, steroids, fatty acids and thyroid hormones around the body, and also plays a significant role in stabilising extracellular fluid[2–4]. It is used medically to treat burns, cerebral bleeding, proteinemia, anaemia, and ascites due to a damaged liver[5,6]. HSA contains multiple binding sites available for metal ions but DAHK, in the N-terminus, shows a higher affinity than the others[7,8]. DAHK can chelate numerous metals such as Cu^{2+}, Ni^{2+} and Co^{2+}, but shows a strong preference for Copper such that it is unlikely to be a viable binding site for other metals[9], and is considered a canonical binding site for Cu(II). Copper binding to DAHK can prevent the formation of Reactive Oxygen Species (ROS), which protects cells from oxidative damage that can eventually lead to neurodegenerative disease, cancers, and respiratory diseases[10]. The chelation of Cu(II) to DAHK instead of amyloid-β can reduce the toxic aggregation of amyloid plaques in the brain, associated with Alzheimer's disease[11,12]. It has also been shown that an analogue of DAHK can improve the restoration of rat hearts from ischemia, indicating possible stroke treatment in the future[1,13]. Therefore, the properties and structure of the Cu-DAHK complex is an important area of research.

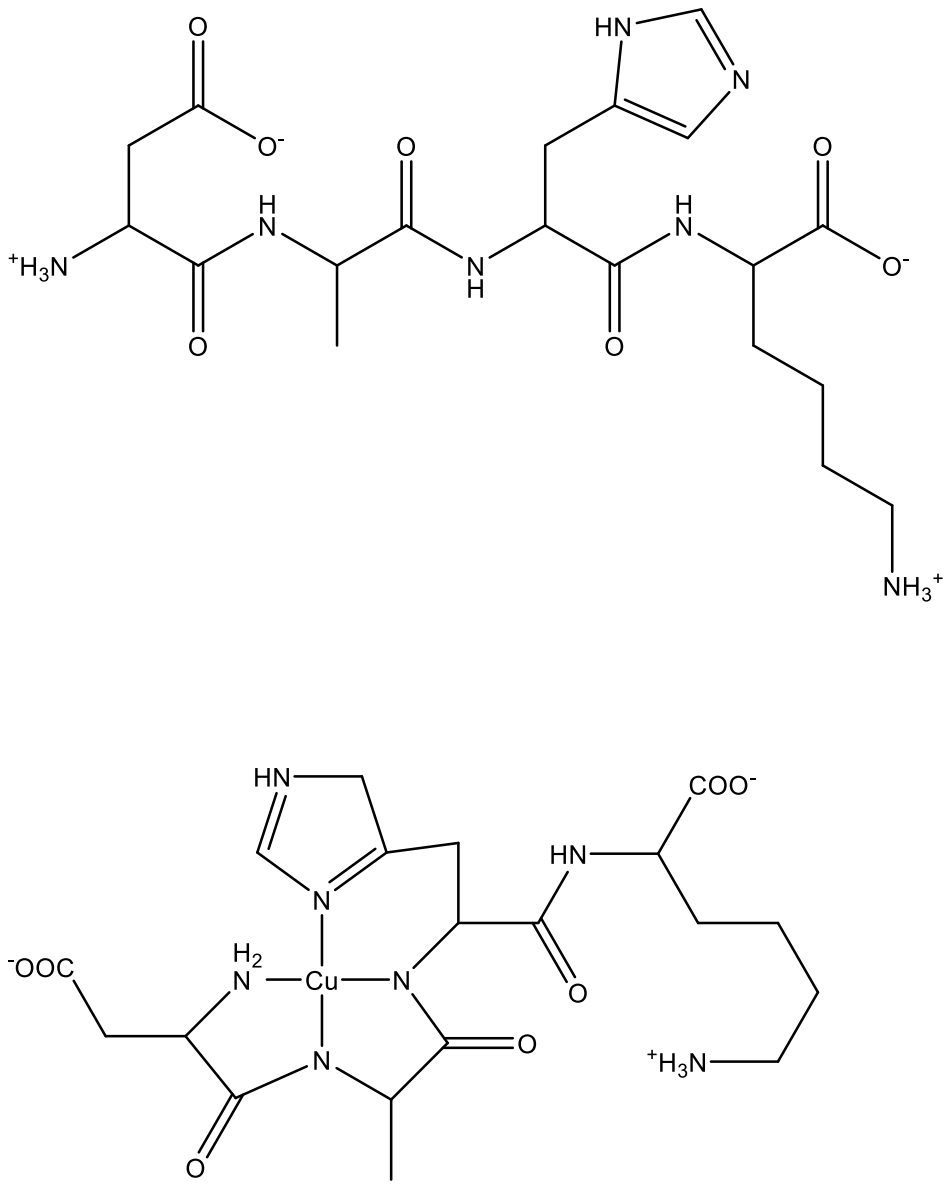

Figure 1 DAHK peptide structure (Asp-Ala-His-Lys) and its complex with Cu(II)

Experimental studies found Cu(II) prefers binding to the Nδ (Nπ in IUPAC notation) of the imidazole ring at biological pH[14], and also coordinates to DAHK via two deprotonated N atoms from the peptide backbone and the terminal NH_2[15] . In addition, X-ray crystallography analysis showed that a water molecule could also bind axially to the Copper, making the Cu(II) five-coordinate. The same study then suggested that prominent features and properties such as the structure and redox activity of the Cu-DAHK peptide, in addition to its biological worth, can be of use as a model for more complex copper-peptide complexes[16]. Computational studies play a major role in studying the structure and function of macromolecules such as proteins and nucleic acids. However, calculations involving metals bound to peptides and

proteins can be complex and computationally expensive. Molecular Mechanics (MM) methods can model large systems, but metal-ligand binding and d-electron effects such as Jahn-Teller distortions[17] are not described in standard MM forcefields. Hybrid QM/MM models are a powerful tool for describing metal-biomolecular systems, but the cost of QM remains an obstacle. The Ligand Field Molecular Mechanics model (LFMM) incorporates a ligand field stabilisation energy (LFSE) term into MM methods to describe d-electron effects[15], and has been used to study small[18,19] and large metalloproteins[20,21] and transition metals such as Cu and Pt [22–27]. Quantum mechanical methods such as DFT are widely used, but challenges such as scale and complexity make calculations laborious. Semi-empirical methods reduce the computational expense dramatically, but they may not describe coordination, covalent and non-covalent interactions in a balanced manner[28]. One recently developed method, GFN2-xTB,[29] is proposed to provide accurate prediction of geometry, frequency and non-covalent interactions for organic and inorganic systems. We recently found excellent performance in describing the interaction of the tripeptide GHK bound to Cu(II)[30]. In addition to our work, several studies used the method on large metal-complexes [31–34]. This paper discusses use of LFMM and GFN2-xTB in predicting the binding mode and conformational preferences of Cu-DAHK, using DFT energies and predictions of spectroscopic data as a benchmark.

Computational Methods

The initial structure of the free peptide DAHK was constructed in extended geometry with each terminus uncapped and in the zwitterionic form using WebMO[35], followed by geometry optimisation using B3LYP-D2[36] with a 6-31G(d)[37] basis set. The Cu(II) ion then was incorporated into the optimised peptide according to a proposed binding site found in the literature[38,39], coordinated to the neutral N-terminus of Asp, Nδ of the His imidazole ring, and deprotonated backbone nitrogens from Asp-Ala and Ala-His, this was optimised using B3LYP-D2/6-31G(d) in the PCM model of aqueous solvent[40]. It should be noted that nitrogens were prepared in protonation state required for metal coordination at this stage, and retained as such throughout all subsequent calculations. Electronic spectra were predicted using time-dependent B3LYP/6-31G(d)/PCM. All DFT calculations were performed in Gaussian09[41]. The DFT-optimised geometry, labelled as “original DFT” below, was used as the starting point for conformational searches. This method was used as a benchmark in previous work[42].

LowModeMD[43] conformational search was carried out using LFMM for Cu(II) and coordinated atoms and the AMBER94 forcefield[44] for the remainder of the peptide. This method, recommended for large and cyclic structures, uses multiple short high-temperature MD simulations to explore conformational space. LFMM calculations were carried out using the DommiMOE extension of the Molecular Operating Environment (MOE)[45]. Bonded MM parameters were explicitly included for Cu-N equatorial ligands, but not for any Cu-O bonds. Charges were assigned as standard library values for organic atoms, and +2.0 on Cu. Conformers found by LFMM were geometry optimised using B3LYP-D2/6-31G(d)/PCM, and also using GFN*2*-xTB with the GB-SA solvent model[46]. Conformational searches were also carried out on Cu-bound and free DAHK using the Conformer-Rotamer Ensemble Sampling Tool (CREST)[32,47,48] implemented within the xTB suite of programs.

Results and discussion

LowModeMD conformational search of free DAHK finished with 123 conformers, whereas CREST gave 88 conformers. In both cases, the lowest energy conformers were significantly more tightly packed (Rg = 3.63 Å) than the initial extended conformer (Rg = 5.25 Å) (full data shown in SI, Table S1) and with five hydrogen bonds, compared to just two in the original DFT structure (Figure 2). Although CREST and LFMM both showed five hydrogen bonds within the molecule, they differ in details: LFMM finds only N-H…O interactions, involving either backbone C=O or the COO^- terminus with either backbone N-H or lysine NH_3. In contrast, CREST finds an N-H…N bond using the lysine side chain and N from the imidazole ring of His, shown in Table 1.

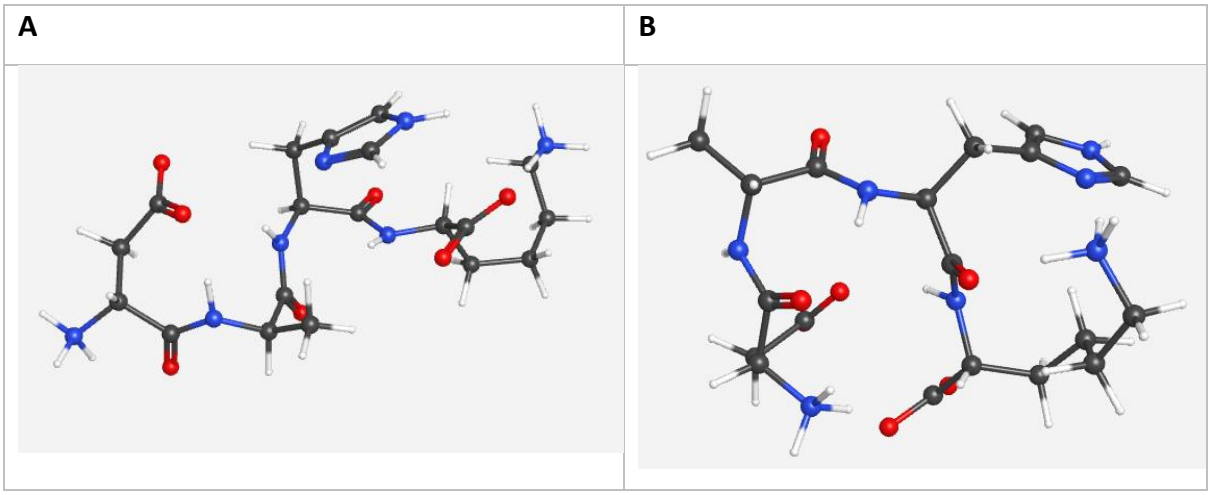

Figure 2 Free peptide DAHK Geometry, where A is the original optimised structure using DFT B3LYP-D2 and B is the lowest energy conformer found via CREST.

Table 1 Comparison of energy and number of hydrogen bonds between the DFT optimised geometry and the lowest energy conformer from LFMM and CREST for free DAHK.

	DFT Energy (Hartree)	Relative E (kJ. mol^{-1})	No. Hydrogen bonds	Rg (Å)
DFT OPT	-1652.74359055	0	2	3.60
LFMM	-1652.78357784	-104.9866	5	3.47
CREST	-1652.75779444	-37.2923	5	3.70

For Cu-DAHK, DFT optimisation results in a distorted square planar geometry around the metal centre, with the shortest bonds to the Nδ of His, the N in the N-terminus, and deprotonated N of Ala-His and Asp-Ala peptide bonds. In addition, the distance between Cu(II) and Asp O, forming the axial 'fifth' coordination optimises to a notably short value (Table 2). Two H-bonds form between NH_3 of Lys and the His and Ala backbone oxygen atoms which may contribute to lowering the energy value of the overall complex (Figure 3).

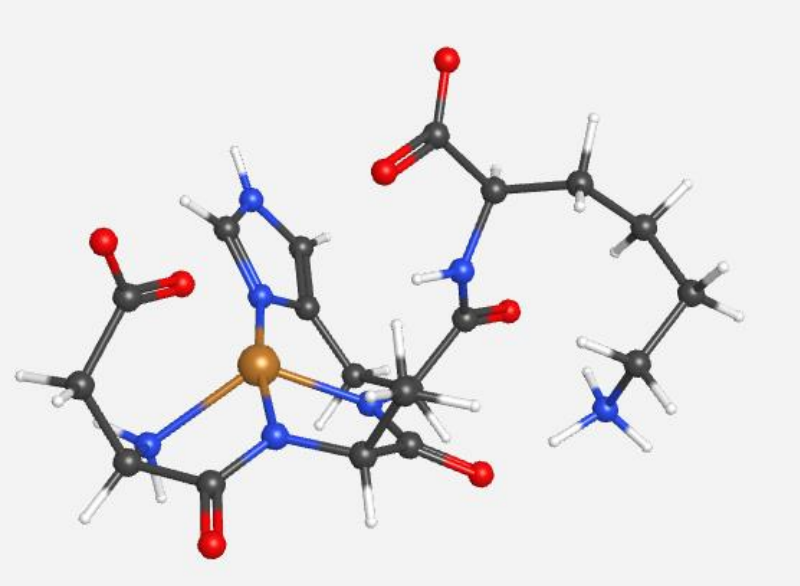

Figure 3 Original DFT structure of Cu-DAHK, optimised at B3LYP-D2/6-31G(d) level.

Table 2 Bond lengths (Å) and angles (°) in the optimised geometry of Cu-DAHK. Using Nδ of the His imidazole ring, the NH_2 backbone and Nd1/ Nd2, the deprotonated nitrogen atoms from the Asp-Ala and Ala-His peptide bonds, respectively.

Distance	Cu-Nδ	Cu-NH2	Cu-Nd2	Cu-Nd1	Cu-ASP O	Cu-LYS O
	1.98	2.01	1.93	2.26	2.03	3.88
Angle	Nδ-Cu-NH2	Nδ-Cu-Nd2	Nδ-Cu-Nd1	NH2-Cu-Nd2	NH2-Cu-Nd1	Nd2-Cu-Nd1
	91.6	171.5	108.6	81.1	123.7	79.2

LFMM LowModeMD conformational search found 11 conformers, *i.e.* less than 10% of those found for free DAHK, showing how Cu binding constrains the conformational flexibility of the peptide. The majority of generated conformers were in a distorted octahedral geometry, with two oxygen atoms in the axial position above and below the Cu-coordination plane, from both the Asp side chain and the C-terminal carboxylate. This geometry is not typical for Cu(II) and differs from the known coordination, this seems to stem from imbalance of d-orbital and non-covalent effects in the LFMM model, and specifically over-estimation of the attraction of the carboxylates to the positive metal centre. However, one conformer (Number 11 in Table S2) is found in a more extended geometry, with four nitrogen ligands in a distorted square planar arrangement around Cu, and a loosely bound axial oxygen from the side chain of Asp. Figure 4 shows the geometry of conformers 1 and 11.

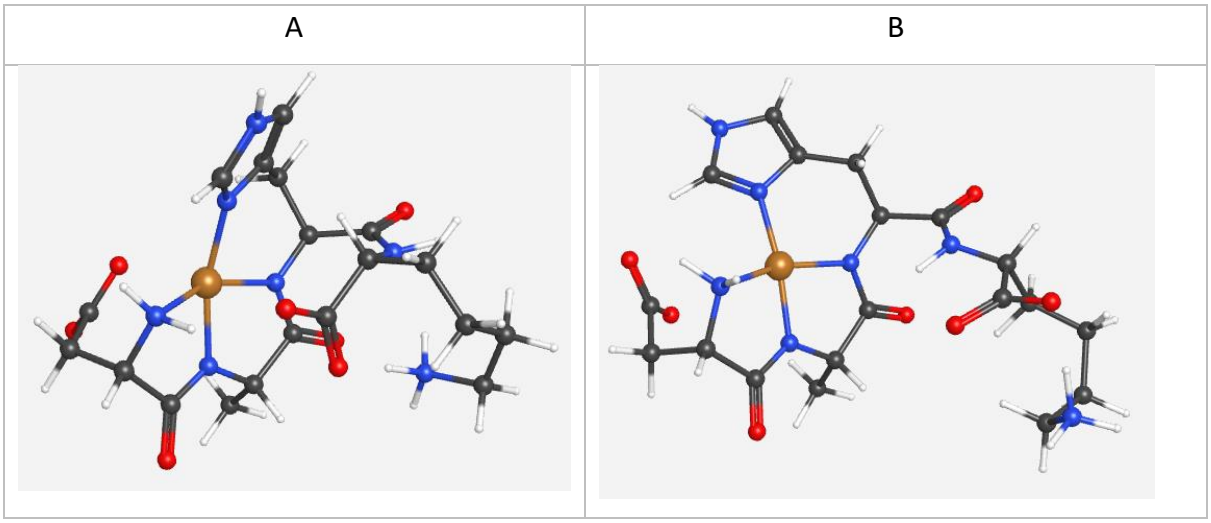

Figure 4 LFMM generated conformers where A is the lowest energy conformer (1), and B is the highest energy (11).

All conformers from LFMM were DFT-optimised, and the relative energy values compared to the original DFT structure. DFT optimisation led to the expected coordination around Cu, with 4 N-ligands in a distorted square planar arrangement with one oxygen in the axial position, with bond lengths and angles remaining within 0.1 Å and 10° of one another. In conformers 1-10, the Asp side chain oxygen shows a Cu-O bond length similar to the other 4 Cu-N bonds. The only conformer that shows a variation in bond angles and lengths is conformer 11, in which Asp does not lend itself as a fifth axial binding site, resulting in a 4N distorted square planar geometry. RMSD values between the LFMM and DFT geometries are typically in the range of 0.5 to 1.5 Å, except conformer 11 which changes by a little over 2 Å. Energies show that the original DFT structure is more stable than most LFMM conformers, with the exception of conformer 10, which is slightly lower in energy than the original DFT geometry (Figure 5 and tables S4 & S5) and also has the lowest Rg value of all conformers. These data indicate that the original DFT geometry provided a reasonable estimation of the Cu-DAHK structure from which to initiate the conformational search, and that the LFMM search efficiently spanned the flexibility of the peptide when bound to Cu. However, subsequent DFT optimisation is required to obtain reliable representation of both geometry and relative energy of conformations.

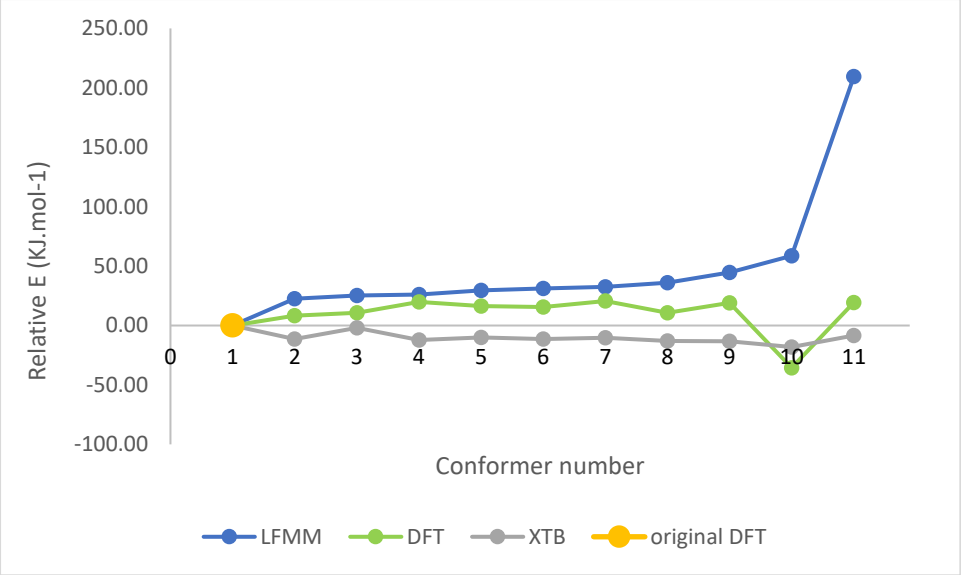

Figure 5 Comparison of relative energies for all conformers using LFMM, DFT and GFN2-xTB against the original DFT structure relative to conformer 1.

Using GFN2-xTB to optimise all eleven DFT conformers also results in conformer 10 being predicted as the lowest energy. In this case, though, conformer 1 is found to be the highest in energy, shown in Table 3 and Figure 6. RMSD values between DFT and xTB are generally below 1 Å, showing that xTB accurately reproduces DFT geometry of most conformers (Figure 6). An exception is conformer 11, for which the absence of an axial ligand increases flexibility. Figure 6 also shows increased RMSD values around 1.5 Å between xTB and LFMM. However, as the RMSD values between DFT and xTB are below 1 Å, this shows that xTB values are the closest to DFT.

Table 3 The GFN2-xTB energies of conformers and the energy relative to conformer 1.

Conformer	xTB Energy (Hartree)	Relative Energy (kJ mol^{-1})
1	-108.30647	0.00
2	-108.31081	-11.39
3	-108.30720	-1.92
4	-108.31109	-12.13
5	-108.31025	-9.92
6	-108.31077	-11.29
7	-108.31041	-10.34
8	-108.31146	-13.10
9	-108.31152	-13.26
10	-108.31336	-18.09
11	-108.30964	-8.32

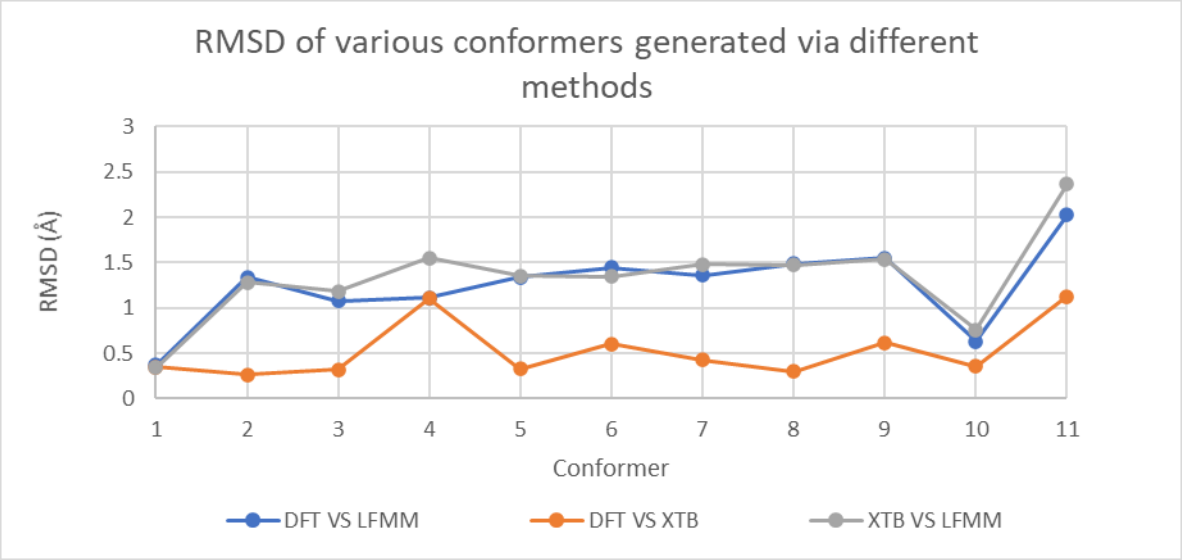

Figure 6 Comparison of RMSD values of all conformers using DFT, LFMM and xTB

The results obtained from the CREST conformational search were significantly different. Taking conformer 1 from LFMM as a starting point 35 conformers were located, this is a much higher value compared to the LFMM equivalent. Repeating the search with different

starting points yielded similar, but not identical, numbers of conformations (Table 4). It was undertaken using four different starting geometries; conformers 1, 2 and 3 generated from LFMM and conformer 10 from DFT. It was found that the results, including number of conformers as well as energy and population of the lowest conformer found, were dependent on starting point.

Table 4 Energy, population and number of conformers found from the different starting points used.

Starting conformer for CREST	Number of conformers found	Population of lowest conformer (%)	Energy of lowest conformer (Hartree)
1	35	90.577	-108.32954
2	41	91.364	-108.32705
3	31	58.995	-108.32942
10	42	94.585	-108.33339

The conformers from CREST showed different binding modes from the original input structures, changing from 4N1O to 3N2O. This stems from replacement of the terminal NH_2 by the Asp carboxylate oxygen in the binding site, and is consistently observed in all such searches. Table 9 shows that the NH_2 bound initially to Cu is completely pushed out in preference for binding to the Asp O. Data for DFT optimisation of each of the lowest energy conformers located by CREST (denoted C1, C2, C3, C10) and selected LFMM conformers (L1, and L2) are reported in Table 5. This shows that the CREST binding mode results in higher energy structures than the expected, literature proposed 4N binding, and considers the amine more stable with a neutral charge forming a distorted square-based pyramid as seen before.

Table 5 Geometry and energy from DFT optimisation of the lowest energy conformers generated via CREST.

Lowest energy conformer	Cu-O Asp bond length (Å)	Cu-NH_2 Asp bond length (Å)	Energy of lowest energy conformer (Hartree)	Energy relative to original DFT structure (kJ/mol)
LFMM/DFT OPTIMISED	2.077	2.197	-3291.46940596	-17.99
C1	1.987	4.782	-3291.44416722	48.28
C2	1.942	4.446	-3291.4639683	-3.71
C3	1.954	4.663	-3291.44374976	49.37
C10	1.959	4.741	-3291.46218136	0.98
L1	1.956	4.657	-3291.44377498	49.31
L2	1.956	4.657	-3291.44377449	49.31

A method of constraint was utilised in CREST whereby the Metal-X bonds are fixed, using conformer 11 as starting point as Asp O in this conformer was not bound to Cu(II). This resulted in the expected 4N binding mode, but with the C-terminal O in the axial position, as shown in Figure 7, rather than the side chain of Asp preferred in all other searches.

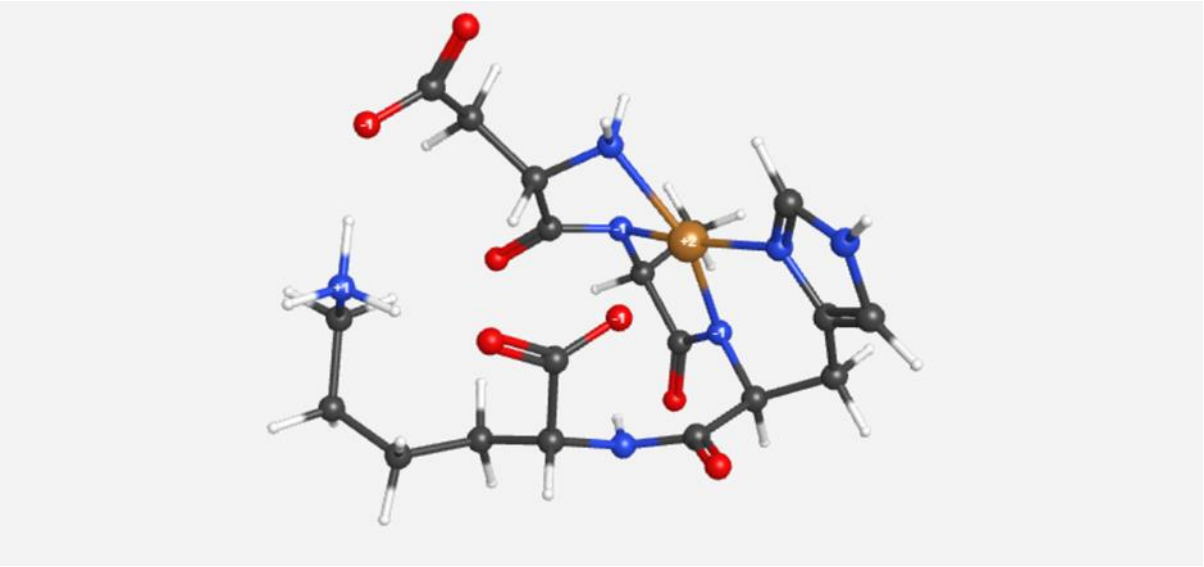

Figure 7 CREST lowest energy conformer found using conformer 11 as a starting point, using constraints around the Copper.

Figure 8 compares the DFT optimised energy of the different binding modes of 4N, 4N1O Asp, 4N1O Lys, 3N1O and 3N2O, relative to the original DFT structure. This confirms that the

original 4N1O binding mode, where O is provided from Asp, is the lowest energy mode. A different 4N1O, with O from Lys is slightly higher in energy. In contrast, the 4N and 3N2O coordination modes are much higher in energy. This result indicates that 4N1O binding modes where oxygen is the axial donor, rather than as part of the distorted square plane, are favoured, and that a four or six-coordinate geometry is highly unlikely.

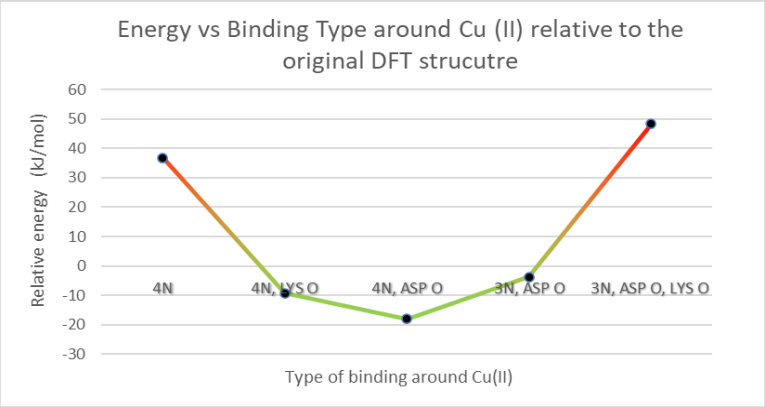

Figure 8 The energies of the different binding modes around Copper, using the lowest energy DFT optimised conformer found in each case, relative to the original DFT structure.

The lowest energy conformations found for each binding mode were used to predict UV-Vis spectra for better comparison against experimental data. Predicted spectra fall into two distinct sets: intense peaks in the range of 250-450 nm, characterised as a ligand to metal charge transfer (LMCT), compare well with literature values of 275 and 307nm, assigned to the NH_2 terminus and the deprotonated amide ligands[16]. The similarity in these bands is expected as the binding around the Copper is the same. The other set contains two weak peaks (one only in the case of 4N) located at around 400-550 nm and 600-700 nm, these are assigned to d-d transitions, and are weaker as they are Laporte forbidden. Literature[16] reports three d-d bands at 490, 520 and 565 nm. The results show a reasonable level of agreement with literature data, although the approximations made in functional, basis set and solvent model mean that exact correspondence is not found.

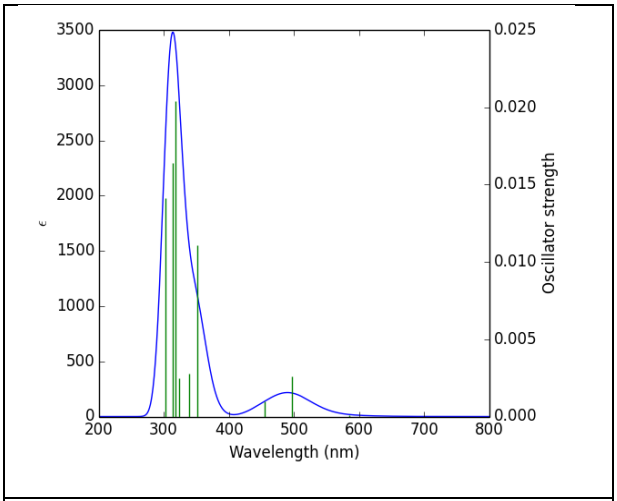

4N (conformer 11) DFT Optimised

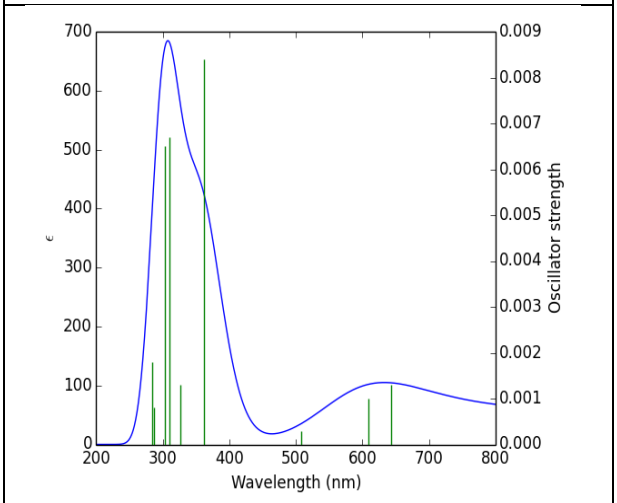

4N1O Asp (conformer 10) DFT Optimised

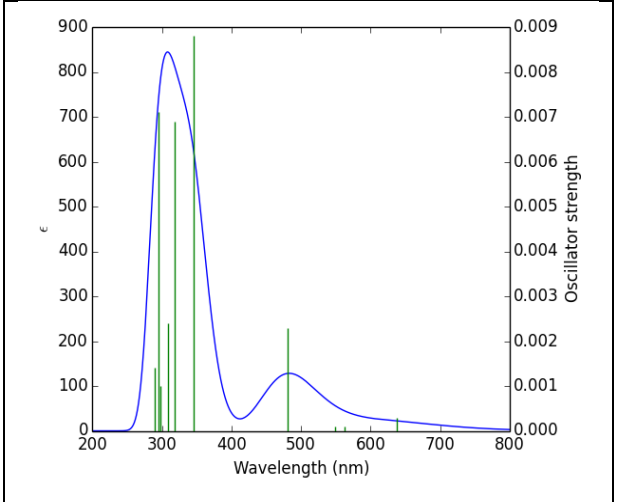

4N1O Lys (conformer 11) from CREST

Figure 9 UV-Vis spectra calculated for different binding modes generated from LFMM/DFT or CREST/DFT.

The 4N binding mode shows only two peaks around 300 and 500 nm, with no noticeable peak at 600-800 nm, whereas the binding modes with O bound to Cu(II) show a third weak peak in the region 600-750 nm as shown in Figure 9. The predicted spectrum of 4N1O Asp shows a broad d-d peak at 642 nm. The 4N1O Lys coordination mode illustrates a similar spectrum to that seen in 4N with d-d peaks at 637 nm and 481 nm. The spectrum of 3N2O Lys found by CREST (shown in SI) is also predicted to have a weak, low energy peak around 800 nm, this is in even less agreement with experiment.

X-ray crystallography data[13] indicated that a water molecule may occupy the axial site: we therefore modelled Cu-DAHK with a water molecule added as an axial ligand. This shows the same 4N distorted square planar geometry about Cu, and hydrogen bonds between water and the side chain of Asp, as shown in Figure 10. The UV-Vis spectra of this structure and free DAHK (Figure 11) show the LMCT transitions in a similar position to Cu-DAHK spectra, with peaks at 295, 313, 325 and 333 nm. However, the d-d transitions are very different to both the simulated spectra and the literature data, at 522, 663 and 773 nm, with the most intense d-d band being seen at 663 nm, a much higher wavelength than the literature value. This might suggest that the crystallographic water is not retained in solution.

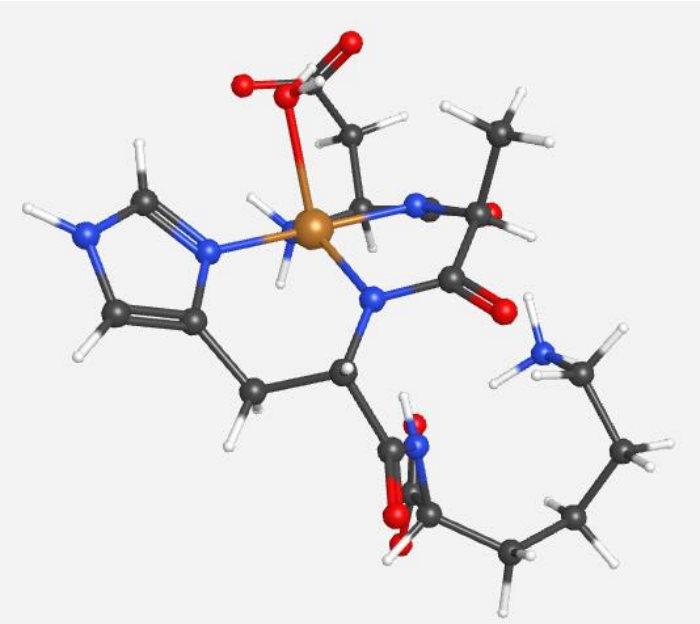

Figure 10 DFT-B3LYP-D2 geometry of 4N binding around copper with an additional water molecule added in the axial position.

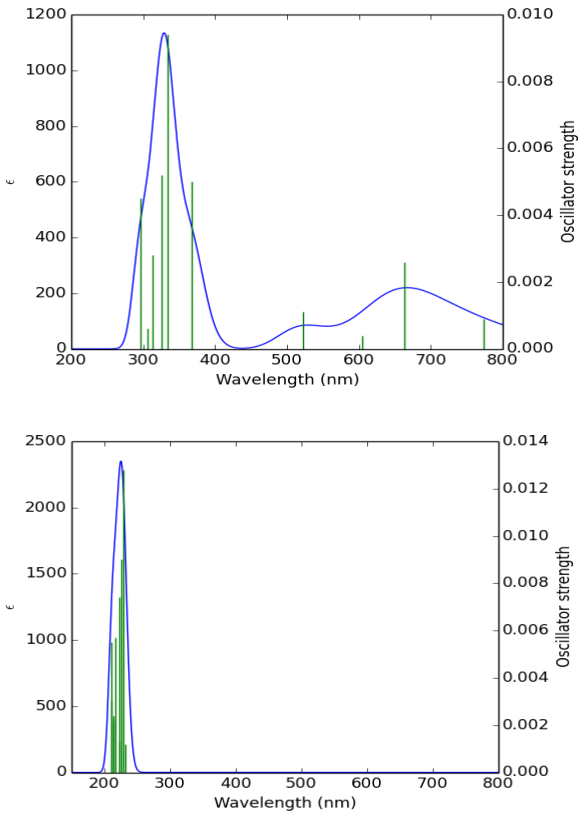

Figure 11 UV-Vis spectrum of DFT optimized Cu-DAHK-H_2O structure (top) and free DAHK (bottom).

Conclusion

The interaction of Cu(II) with the tetrapeptide DAHK, which makes up the N-terminus of human serum albumin has been investigated theoretically. Ligand Field Molecular Mechanics (LFMM), DFT and semi-empirical methods have been used to examine the Copper binding mode and peptide conformation, the latter was explored using LowModeMD searching within an MM framework, as well as the conformational-rotational estimation tool (CREST) within the semi-empirical method GFN2-xTB. Suitable sampling methods successfully predicted low energy structures compared to the original DFT structure constructed manually. LFMM conformational search resulted in 11 conformers and described the binding modes similarly to that of the literature, however showed a preference for two axial oxygen donors. DFT and GFN2-xTB geometry optimisation correctly produced the expected 4N1O Asp binding in all conformers but one. In contrast, CREST conformational search changed the Cu coordination to 3N2O unless metal-ligand bonds were constrained to remain attached throughout. In this

case, 4N1O coordination was correctly predicted, but with Lys providing the axial O donor rather than Asp.

4N1O was found to be the lowest energy of the five binding modes obtained from all conformational searches, with a slight preference for Asp in the axial position over Lys. Other binding modes, including 4N with no axial ligand or 3N2O, are much higher in energy. Prediction of UV-Vis spectra showed that the 4N binding mode possessed the most similar UV spectrum to the literature; this suggests the axial position could be left free for a water molecule rather than using oxygen within the molecule. However, the predicted spectrum for CuDAHK-H_2O differs markedly from the literature. This suggests the axial oxygen is not strongly bound and is more fluxional, a situation that is supported by the long Cu-OH_2 bond length reported in the literature.

In summary, we have set out a protocol for prediction of the structure of Cu bound to a tetrapeptide. LFMM conformational search followed by either DFT or GFN2-xTB geometry optimisation in simulated water solvent yields excellent agreement with the literature binding mode. Any one method alone does not yield the correct structure: LFMM alone predicts six-coordinate structures, while GFN2-xTB favours 3N2O coordination over the correct 4N1O. Dispersion corrected DFT works well, but is too computationally demanding to use as the basis of a conformational search. The multiscale approach taken here is an accurate and computationally efficient means to tackle this, and related bio-inorganic systems.

Acknowledgements

Nadiyah Alshammari thanks the ministry of education, Kingdom of Saudi Arabia for the provision of a PhD scholarship and support. We are grateful to Advanced Research Computing at Cardiff (ARCCA) and Supercomputing Wales for access to computing resources.

Reference

1 E. T. Gum, R. A. Swanson, C. Alano, J. Liu, S. Hong, P. R. Weinstein and S. S. Panter, Human Serum Albumin and its N-Terminal Tetrapeptide (DAHK) Block Oxidant-Induced Neuronal Death, *Stroke*, 2004, **35**, 590–595.

2 M. Anraku, K. Yamasaki, T. Maruyama, U. Kragh-Hansen and M. Otagiri, Effect of Oxidative Stress on the Structure and Function of Human Serum Albumin, *Pharm. Res.*, 2001, **18**, 632–639.

3 E. Tsuchida, K. Sou, A. Nakagawa, H. Sakai, T. Komatsu and K. Kobayashi, Artificial oxygen carriers, hemoglobin vesicles and albumin-hemes, based on bioconjugate chemistry, *Bioconjug. Chem.*, 2009, **20**, 1419–1440.

4 Y. He, T. Ning, T. Xie, Q. Qiu, L. Zhang, Y. Sun, D. Jiang, K. Fu, F. Yin, W. Zhang, L. Shen, H. Wang, J. Li, Q. Lin, Y. Sun, H. Li, Y. Zhu and D. Yang, Large-scale production of functional human serum albumin from transgenic rice seeds, *Proc. Natl. Acad. Sci. U. S. A.*, 2011, **108**, 19078–19083.

5 M. R. Alexander, J. J. Ambre, B. I. Liskow and D. C. Trost, *Therapeutic Use of Albumin*, .

6 G. Hastings, P. W.-A. of family medicine and undefined 1992, The therapeutic use of albumin., *europepmc.org*.

7 W. Bal, M. Sokołowska, E. Kurowska and P. Faller, *Biochim. Biophys. Acta - Gen. Subj.*, 2013, 1830, 5444–5455.

8 U. Kragh-Hansen, *Dan. Med. Bull.*, 1990, 37, 57–84.

9 M. Sokołowska, M. Wszelaka-Rylik, J. Poznański and W. Bal, Spectroscopic and thermodynamic determination of three distinct binding sites for Co(II) ions in human serum albumin, *J. Inorg. Biochem.*, 2009, **103**, 1005–1013.

10 Z. Liu, Z. Ren, J. Zhang, C. C. Chuang, E. Kandaswamy, T. Zhou and L. Zuo, Role of ROS and nutritional antioxidants in human diseases, *Front. Physiol.*, 2018, **9**, 1–14.

11 C. D. Syme, R. C. Nadal, S. E. J. Rigby and J. H. Viles, Copper binding to the amyloid-β (aβ) peptide associated with Alzheimer's disease: Folding, coordination geometry, pH dependence, stoichiometry, and affinity of Aβ-(1-28): Insights from a range of complementary spectroscopic techniques, *J. Biol. Chem.*, 2004, **279**, 18169–18177.

12 L. Perrone, E. Mothes, M. Vignes, A. Mockel, C. Figueroa, M. C. Miquel, M. L. Maddelein and P. Faller, Copper transfer from Cu-Aβ to human serum albumin inhibits aggregation, radical production and reduces Aβ toxicity, *ChemBioChem*, 2010, **11**, 110–118.

13 F. J. Sutherland, D. Bar-Or, C. G. Curtis and D. J. Hearse, Attenuation of trace element-mediated injury during ischemia and reperfusion by an N-terminus analogue of human albumin (H4DUS60131), *J. Cardiovasc. Pharmacol.*, 2002, **39**, 722–728.

14 M. Sokolowska, A. Krezel, M. Dyba, Z. Szewczuk and W. Bal, Short peptides are not reliable models of thermodynamic and kinetic properties of the N-terminal metal binding site in serum albumin, *Eur. J. Biochem.*, 2002, **269**, 1323–1331.

15 A. Schirer, Y. El Khoury, P. Faller, P. Hellwig, Y. El Khoury, P. Faller, P. Hellwig, Y. El Khoury, P. Faller and P. Hellwig, Similarities and differences of copper and zinc cations binding to biologically relevant peptides studied by vibrational spectroscopies, *JBIC J. Biol. Inorg. Chem.*, 2017, **22**, 581–589.

16 C. Hureau, H. Eury, R. Guillot, C. Bijani, S. Sayen, P.-L. P. Solari, E. Guillon, P. Faller and P. Dorlet, X-ray and Solution Structures of CuIIGHK and CuIIDAHK Complexes: Influence on Their Redox Properties, *Chem. - A Eur. J.*, 2011, **17**, 10151–10160.

17 R. J. Deeth, The ligand field molecular mechanics model and the stereoelectronic effects of d and s electrons, *Coord. Chem. Rev.*, 2001, **212**, 11–34.

18 R. J. Deeth and L. J. A. Hearnshaw, Molecular modelling of Jahn–Teller distortions in Cu(ii)N6 complexes: elongations{,} compressions and the pathways in between, *Dalt. Trans.*, 2006, 1092–1100.

19 R. J. Deeth and L. J. A. Hearnshaw, Molecular modelling for coordination compounds: Cu(ii)–amine complexes, *Dalt. Trans.*, 2005, 3638–3645.

20 R. J. Deeth, A test of ligand field molecular mechanics as an efficient alternative to QM/MM for modelling metalloproteins: the structures of oxidised type I copper centres, *Chem. Commun.*, 2006, 2551–2553.

21 H. Do, R. J. Deeth and N. A. Besley, Computational Study of the Structure and Electronic Circular Dichroism Spectroscopy of Blue Copper Proteins, *J. Phys. Chem. B*, 2013, **117**, 8105–8112.

22 M. Turner, J. A. Platts and R. J. Deeth, Modeling of Platinum-Aryl Interaction with Amyloid-β Peptide, *J. Chem. Theory Comput.*, 2016, **12**, 1385–1392.

23 M. Turner, S. T. Mutter, R. J. Deeth and J. A. Platts, Ligand field molecular dynamics simulation of Pt(II)-phenanthroline binding to N-terminal fragment of amyloid-beta peptide, *PLoS One*, 2018, **13**, e0193668.

24 S. T. Mutter, M. Turner, R. J. Deeth and J. A. Platts, Metal Binding to Amyloid-β1–42: A Ligand Field Molecular Dynamics Study, *ACS Chem. Neurosci.*, 2018, **9**, 2795–2806.

25 M. Ćendić, Z. D. Matović and R. J. Deeth, Molecular modeling for Cu(II)-aminopolycarboxylate complexes: Structures, conformational energies, and ligand binding affinities, *J. Comput. Chem.*, 2013, **34**, 2687–2696.

26 A. Bentz, P. Comba, R. J. Deeth, M. Kerscher, B. Seibold and H. Wadepohl, Modeling of the Various Minima on the Potential Energy Surface of Bispidine Copper(II) Complexes: A Further Test for Ligand Field Molecular Mechanics, *Inorg. Chem.*, 2008, **47**, 9518–9527.

27 H. C. Tai, R. Brodbeck, J. Kasparkova, N. J. Farrer, V. Brabec, P. J. Sadler and R. J. Deeth, Combined theoretical and computational study of interstrand DNA guanine-guanine cross-linking by trans -[Pt(pyridine) 2] derived from the photoactivated prodrug trans,trans,trans -[Pt(N 3) 2(OH) 2(pyridine) 2], *Inorg. Chem.*, 2012, **51**, 6830–6841.

28 C. J. Cramer, *Essentials of Computational Chemistry Theories and Models Second*

Edition, 2004.

29 C. Bannwarth, S. Ehlert and S. Grimme, GFN2-xTB—An Accurate and Broadly Parametrized Self-Consistent Tight-Binding Quantum Chemical Method with Multipole Electrostatics and Density-Dependent Dispersion Contributions, *J. Chem. Theory Comput.*, 2019, **15**, 1652–1671.

30 N. Alshammari and J. A. J. A. Platts, Theoretical Study of Copper binding to GHK peptide, *Comput. Biol. Chem.*, 2020, **86**, 107265.

31 M. Bursch, H. Neugebauer and S. Grimme, Structure Optimisation of Large Transition-Metal Complexes with Extended Tight-Binding Methods, *Angew. Chemie Int. Ed.*, 2019, **58**, 11078–11087.

32 S. Grimme, Exploration of Chemical Compound, Conformer, and Reaction Space with Meta-Dynamics Simulations Based on Tight-Binding Quantum Chemical Calculations, *J. Chem. Theory Comput.*, 2019, **15**, 2847–2862.

33 A. Kovács, J. Cz. Dobrowolski, S. Ostrowski and J. E. Rode, Benchmarking density functionals in conjunction with Grimme's dispersion correction for noble gas dimers (Ne2, Ar2, Kr2, Xe2, Rn2), *Int. J. Quantum Chem.*, 2017, **117**, e25358.

34 M. Bursch, A. Hansen and S. Grimme, Fast and Reasonable Geometry Optimization of Lanthanoid Complexes with an Extended Tight Binding Quantum Chemical Method, *Inorg. Chem.*, 2017, **56**, 12485–12491.

35 WebMO v19.0.009e, www.webmo.net.

36 C. Lee, W. Yang and R. G. Parr, Development of the Colle-Salvetti correlation-energy formula into a functional of the electron density, *Phys. Rev. B*, 1988, **37**, 785–789.

37 V. A. Rassolov, M. A. Ratner, J. A. Pople, P. C. Redfern and L. A. Curtiss, 6-31G* basis set for third-row atoms, *J. Comput. Chem.*, 2001, **22**, 976–984.

38 A. Schirer, Y. El Khoury, P. Faller and P. Hellwig, Similarities and differences of copper and zinc cations binding to biologically relevant peptides studied by vibrational spectroscopies, *JBIC J. Biol. Inorg. Chem.*, 2017, **22**, 581–589.

39 C. Hureau, H. Eury, R. Guillot, C. Bijani, S. Sayen, P. L. Solari, E. Guillon, P. Faller and P.

Dorlet, X-ray and solution structures of Cu IIGHK and Cu IIDAHK complexes: Influence on their redox properties, *Chem. - A Eur. J.*, 2011, **17**, 10151–10160.

40 B. Mennucci, *Wiley Interdiscip. Rev. Comput. Mol. Sci.*, 2012, 2, 386–404.

41 Gaussian09 Rev D.01 Frisch, M. J.; Trucks, G. W.; Schlegel, H. B.; Scuseria, G. E.; Robb, M. A.; Cheeseman, J. R.; Scalmani, G.; Barone, V.; Mennucci, B.; Petersson, G. A.; Nakatsuji, H.; Caricato, M.; Li, X.; Hratchian, H. P.; Izmaylov, A. F.; Bloino, J.; Zheng, G.; Sonnenb, 2009.

42 S. T. Mutter, R. J. Deeth, M. Turner and J. A. Platts, Benchmarking of copper(II) LFMM parameters for studying amyloid- peptides, *J. Biomol. Struct. Dyn.*, 2018, **36**, 1145–1153.

43 P. Labute, LowModeMD—Implicit Low-Mode Velocity Filtering Applied to Conformational Search of Macrocycles and Protein Loops, *J. Chem. Inf. Model.*, 2010, **50**, 792–800.

44 W. D. Cornell, P. Cieplak, C. I. Bayly, I. R. Gould, K. M. Merz, D. M. Ferguson, D. C. Spellmeyer, T. Fox, J. W. Caldwell and P. A. Kollman, A Second Generation Force Field for the Simulation of Proteins, Nucleic Acids, and Organic Molecules, *J. Am. Chem. Soc.*, 1995, **117**, 5179–5197.

45 Molecular Operating Environment (MOE) (2014) Chemical Computing Group Inc. and Https://www.chemcomp.com/, 2013.

46 H. Nguyen, D. R. Roe and C. Simmerling, Improved generalized born solvent model parameters for protein simulations, *J. Chem. Theory Comput.*, 2013, **9**, 2020–2034.

47 S. Grimme, C. Bannwarth, S. Dohm, A. Hansen, J. Pisarek, P. Pracht, J. Seibert and F. Neese, Fully Automated Quantum-Chemistry-Based Computation of Spin–Spin-Coupled Nuclear Magnetic Resonance Spectra, *Angew. Chemie Int. Ed.*, 2017, **56**, 14763–14769.

48 P. Pracht, F. Bohle and S. Grimme, Automated exploration of the low-energy chemical space with fast quantum chemical methods, *Phys. Chem. Chem. Phys.*, 2020, **22**.